ACS Catalysis

pubs.acs.org/acscatalysis Research Article

Photoelectrochemical Urea Synthesis from Nitrate and Carbon Dioxide on GaN Nanowires

Wan Jae Dong,[§] Jan Paul Menzel,[§] Zhengwei Ye, Ishtiaque Ahmed Navid, Peng Zhou, Ke R. Yang, Victor S. Batista,* and Zetian Mi*

Cite This: *ACS Catal.* 2024, 14, 2588–2596 Read Online

ACCESS | Metrics & More | Article Recommendations | Supporting Information

ABSTRACT: Semiconductor photoelectrodes can be used to synthesize urea from carbon dioxide and nitrate under solar light. We find that GaN nanowires (NWs) have inherent catalytic activity for nitrate conversion to nitrite, while Ag cocatalysts loaded onto GaN NWs further promote the performance of photoelectrochemical urea synthesis. Under optimized conditions, a high faradaic efficiency of 75.6 ± 2.6% was achieved at a potential of −0.3 vs reversible hydrogen electrode. Control experiments and theoretical calculations suggest that the high selectivity of urea originates from the facilitated C−N coupling between key intermediates of NO_2 and COO^- at an early stage of the reduction reaction. This work demonstrates the potential of GaN NWs with loaded Ag cocatalysts to achieve solar-powered urea synthesis with an efficiency higher than that of previously reported methods.

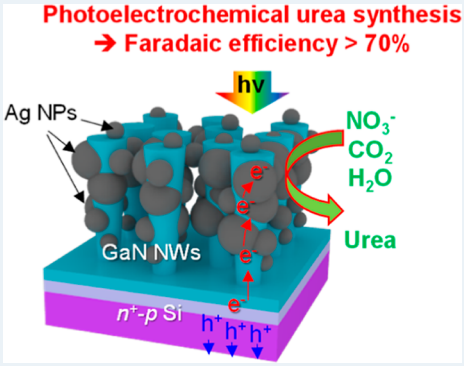

KEYWORDS: *urea, nitrate reduction, carbon dioxide reduction, GaN, photoelectrode, metal cocatalyst*

Downloaded via YALE UNIV on March 5, 2024 at 22:50:34 (UTC).
See https://pubs.acs.org/sharingguidelines for options on how to legitimately share published articles.

1. INTRODUCTION

Sustainable carbon and nitrogen recycling has emerged as a critical energy and environmental issue as we move toward a future with zero carbon emissions. Electrochemical carbon dioxide (CO_2) reduction reaction is a promising route for reducing CO_2 emission and producing value-added chemicals such as CO, HCOOH, CH_4, and multicarbon products.[1−4] The development of electrocatalysts for CO_2 reduction reactions has enabled the selective production of target chemicals in aqueous electrolytes. There are two main pathways for nitrogen recycling, including nitrogen (N_2)[5−7] or nitrate (NO_3^-) reduction reactions[8−11] to ammonia (NH_3), an essential raw material for modern chemistry. Both reactions offer a clean method for NH_3 synthesis compared to the conventional, energy-intensive, and carbon-emitting Haber−Bosch process.[12,13] NO_3^- reduction is thermodynamically more feasible than N_2 reduction because the N═O bond has much lower dissociation energy (204 kJ/mol) than the N≡N bond (941 kJ/mol), and NO_3^- is about 40,000 times more soluble in water than N_2.[11,14] Therefore, high selectivity and productivity of NH_3 have been achieved by electrochemical NO_3^- reduction using various electrocatalysts.[9,15,16]

Urea [$CO(NH_2)_2$] is an essential fertilizer manufactured through a two-step process under high-temperature and high-pressure conditions. The Haber−Bosch process first yields NH_3, as depicted in the following chemical reaction: $N_2 + 3H_2 \rightarrow 2NH_3$. Subsequently, NH_3 reacts with CO_2 to produce urea, following the chemical equation: $2NH_3 + CO_2 \rightarrow CO(NH2)_2 + H_2O$.[17−19] Recently, the electrochemical synthesis of urea has been demonstrated by simultaneous CO_2 reduction and $N_2/NO/NO_2^-/NO_3^-$ reduction at room temperature and under ambient pressure. For instance, PdCu−TiO_2,[20] Bi−$BiVO_4$ heterostructure,[21] CuPc nanotubes,[22] InOOH nanoparticles (NPs),[23] and polypyrrole-coated Pt electrode[24] produced urea from direct coupling of N_2 with CO_2. However, the faradaic efficiency (FE_{urea}) has remained lower than 20% due to the difficulty of activating N_2. As alternatives to nitrogen sources, NO and NO_2^- have been electrochemically converted to urea with higher FE_{urea} (11−43%) using Zn nanobelts,[25] Te−Pd nanocrystals,[26] ZnO nanosheets,[27] and Cu−TiO_2 catalysts.[28] More recently, oxygen-vacancy-enriched CeO_2,[29] $In(OH)_3$,[30] and InOOH[31] catalysts as well as TiO_2-Nafion,[32] Cu−Zn nanowires (NWs),[33] Fe−Ni diatomic catalysts,[34] and Cu−N−C single-atom catalysts[35] have enabled the concurrent reduction of NO_3^- and CO_2 to urea in aqueous electrolyte. In particular, experiments with $In(OH)_3$ and InOOH have achieved high selectivity of urea generation (FE_{urea} > 50%) at cathodic potentials of −0.6 and −0.5 V versus the reversible hydrogen electrode (V_{RHE}), respectively.[30,31] Theoretical

Received: September 9, 2023
Revised: January 14, 2024
Accepted: January 22, 2024
Published: February 5, 2024

© 2024 American Chemical Society

https://doi.org/10.1021/acscatal.3c04264
ACS Catal. 2024, 14, 2588−2596

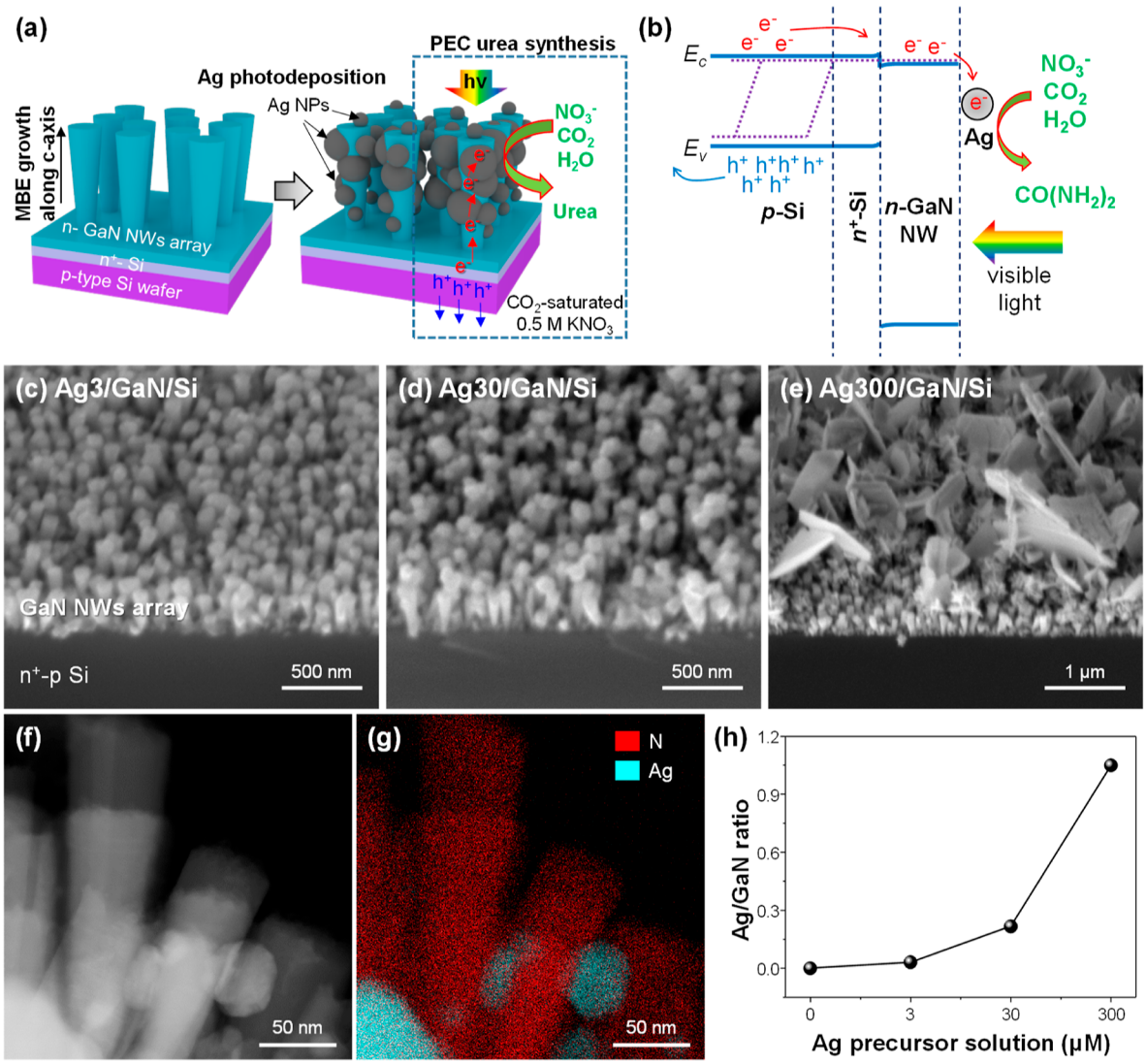

Figure 1. (a) Schematic fabrication process of Ag NP-loaded GaN NWs vertically grown on the n^+−p Si photoelectrode. PEC urea synthesis was conducted under solar light with cathodic bias. (b) Energy band diagram of the Ag/GaN/Si photoelectrode under light illumination. Photoexcited electrons migrate from Si to Ag NPs through GaN NWs and participate in urea synthesis in an aqueous solution containing NO_3^- and CO_2. (c−e) Tilt-view SEM images of Ag/GaN/Si photoelectrodes with different loading amounts of Ag cocatalysts. The loading amount of Ag was controlled by adjusting the molar concentration of $AgNO_3$ precursor solution during the photodeposition step. (f) HAADF-STEM image and (g) EDS elemental map of Ag30/GaN NWs. (h) Surface Ag/GaN ratio obtained from XPS measurement.

calculations have suggested that the facilitated C−N coupling between $*NO_2^-$ and $*CO_2$ intermediates on $In(OH)_3$ at an early stage of the reaction can promote urea synthesis more effectively than the conventional C−N coupling between $*NH_2$ and *CO. Furthermore, rational design of the Cu−W bimetallic C−N coupling sites improved the performance of electrocatalysts, resulting in high FE_{urea} > 70%.[36] However, the applied potential in electrochemical urea synthesis is still needed, and the product selectivity is still much lower than that of the individual CO_2-to-CO and NO_3^--to-NH_3 conversion reactions, which typically show faradaic efficiency above 80%.

This bottleneck in the electrochemical method can be mitigated by developing a photoelectrode. Semiconductor photoelectrodes generate a built-in potential under solar light, which can be used to shift the operating potential to a more positive value. This has been demonstrated in photoelectrodes for hydrogen evolution[37−40] and CO_2 reduction reactions.[41−44] However, there has been no demonstration of any photoelectrode for urea synthesis to our knowledge. Therefore, there is an urgent need to screen semiconductor materials, understand their catalytic mechanisms, and optimize the physical and chemical structures for enhancing the performance of photoelectrochemical (PEC) urea synthesis. Semiconductor materials capable of efficiently and stably producing urea in aqueous electrolytes hold great promise as advanced photocatalysts for solar-driven urea production.

In this work, we found that GaN NWs grown on n^+−p Si photoelectrodes exhibit catalytic activity for urea synthesis. An unprecedented high FE_{urea} of 74.5 ± 4.1% was achieved at −0.3 V_{RHE} by concurrent NO_3^- and CO_2 reduction reactions. More noticeably, when Ag cocatalysts were loaded onto GaN NWs, the onset potential was positively shifted by ∼0.1 V and the potential range for selective urea production (FE_{urea} > 45%) was significantly broadened. This resulted in a 4-fold increase in the urea production rate (4.4 ± 0.9 $\mu mol/cm^2/h$) at −0.6 V_{RHE}. Control experiments and theoretical calculations

https://doi.org/10.1021/acscatal.3c04264
ACS Catal. 2024, 14, 2588−2596

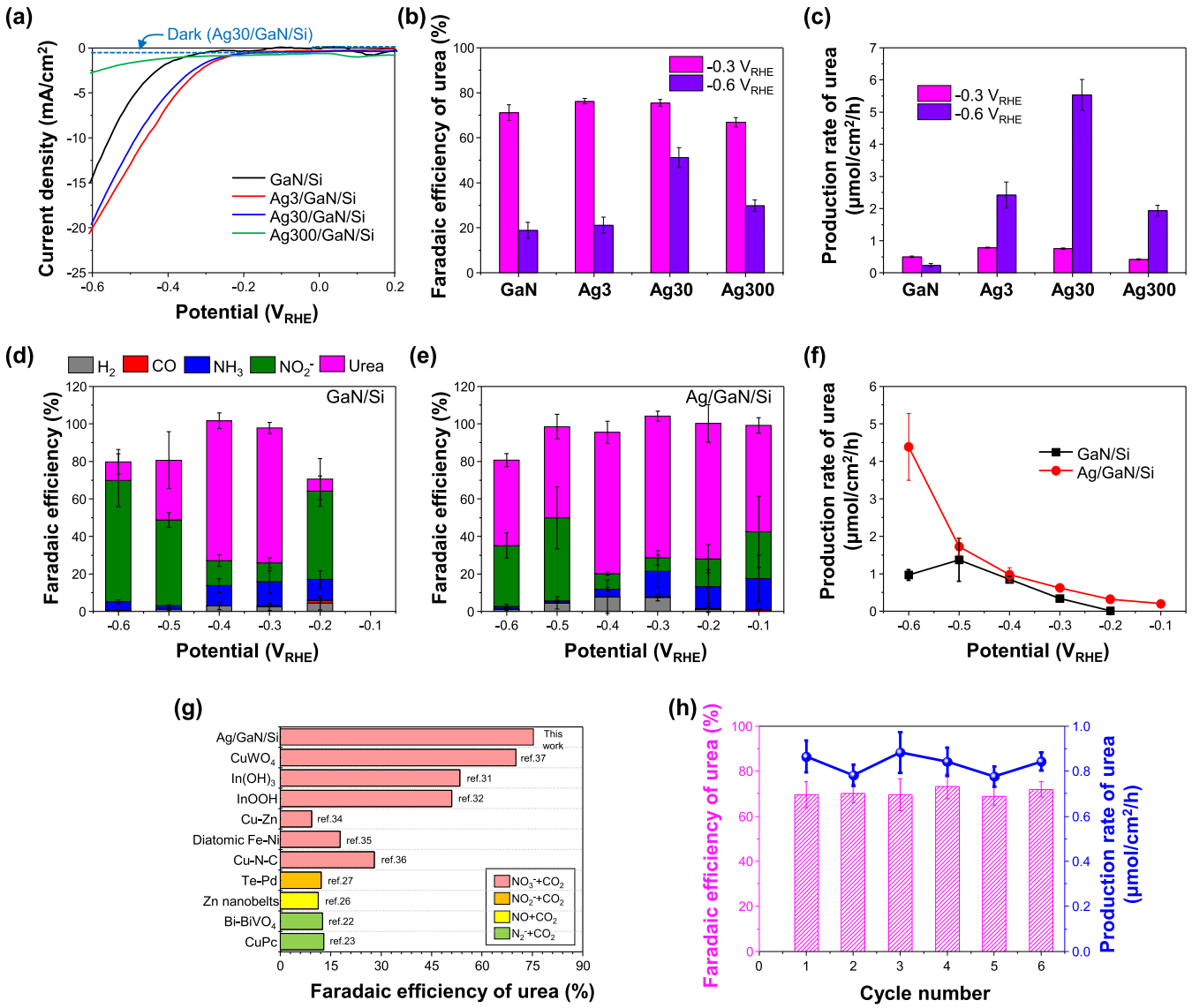

Figure 2. (a) LSV curves, (b) faradaic efficiency, and (c) production rate for GaN/Si, Ag3/GaN/Si, Ag30/GaN/Si, and Ag300/GaN/Si photoelectrodes. The product analysis was conducted at −0.3 and −0.6 V_{RHE} in CO_2-saturated 0.5 M KNO_3 aqueous electrolyte under AM 1.5 G-filtered 1 sun. Faradaic efficiency at different potentials for (d) GaN/Si and (e) Ag/GaN/Si. (f) Urea production rate of GaN/Si and Ag/GaN/Si at different potentials. The measurements were performed 4 times. (g) Comparison of FE_{urea} between the Ag/GaN/Si photoelectrode and previously reported electrocatalysts. (h) Stability test of Ag30/GaN/Si at −0.3 V_{RHE}. Each cycle was conducted for 1 h.

suggested that the GaN surface effectively produced NO_2 intermediates, which then interacted with COO^- radicals and resulted in C−N coupling at the early stage of urea synthesis. This study shows that GaN can selectively produce urea by promoting C−N bonds from the NO_3^- and CO_2.

2. RESULTS AND DISCUSSION

2.1. Ag Cocatalysts on GaN NWs/n⁺−p Si Photoelectrodes. N-type GaN NWs were vertically grown along the *c*-axis of the wurtzite crystal on an n^+−p Si wafer by plasma-assisted molecular beam epitaxy under nitrogen-rich conditions (Figure 1a). Ag NP cocatalysts were then loaded onto the GaN NWs by photodeposition as described in the Experimental Section. When the photoelectrode is irradiated with light, the photoexcited electrons in the Si wafer move toward the GaN NWs and the Ag cocatalysts due to the built-in potential of the n^+−p Si junction and the applied cathodic bias. The photogenerated electrons can migrate to GaN and Ag surfaces without significant electrical resistance (Figure 1b) since there is negligible energy offset between the conduction bands of n^+-Si and n-GaN while the work function of Ag is below the conduction band edge of n-GaN.[38,45] Subsequently, the electrons on the surfaces of GaN and Ag participate in the reduction steps that synthesize urea from the NO_3^- and CO_2 under aqueous conditions.

We prepared three different Ag/GaN/Si photoelectrodes by changing the molar concentration of $AgNO_3$ precursor solution used for photodeposition and denoted them as Ag#/GaN/Si, where # is the molar concentration of $AgNO_3$ in the unit of μM. As the amount of Ag precursor solution increased from 3 to 300 μM, the size of Ag cocatalysts became larger on GaN NWs (Figure 1c−e). In the case of Ag3 and Ag30, small NPs were formed on GaN NWs, whereas in Ag300, large microscale plate-shaped Ag particles were grown on the GaN surface. This indicates that the morphology and surface coverage of Ag cocatalysts, which are closely related to

https://doi.org/10.1021/acscatal.3c04264
ACS Catal. 2024, 14, 2588−2596

the photocurrent generation of the underlying GaN/Si photoelectrode and catalytic performance for urea synthesis, can be well-controlled. The microstructure of Ag30/GaN NWs was characterized using high-angle annular dark-field scanning transmission electron microscopy (HAADF-STEM) after the Ag/GaN NW array was scraped from the Si wafer (Figures 1f and S1). Ag NPs ranging in size from 10 to 80 nm were observed on GaN NWs with a length of ∼400 nm and a diameter of ∼50 nm. The elemental distribution of N (red) from GaN NWs and Ag (cyan) from Ag NPs was investigated by energy-dispersive X-ray spectroscopy (EDS) (Figure 1g). The N element was uniformly distributed over the GaN NWs, whereas Ag NPs were partially covered on the GaN surface. The area ratio of Ag NPs to GaN NWs was measured to be approximately 0.19, providing an estimate of the surface coverage of Ag NPs on GaN NWs (Figure S2a). In the high-resolution STEM images, Ag(111) planes with a *d*-spacing of 0.235 nm were predominantly observed (Figure S2b−d). The X-ray diffraction (XRD) patterns showed a prominent GaN (002) peak, indicating the presence of single-crystalline GaN NWs across all samples (Figure S3). Notably, the XRD pattern corresponding to Ag NPs was absent in Ag3/GaN/Si. However, a peak of Ag(111) emerged in Ag30/GaN/Si, becoming more pronounced in Ag300/GaN/Si due to the increased crystallite size and density of Ag NPs.

The surface bonding states of cocatalysts were characterized by X-ray photoelectron spectroscopy (XPS) analysis (Figure S4). Ag3/GaN/Si exhibited a minor Ag^+ state alongside a major Ag^0 state (Figure S5). Notably, the Ag^+ bonding state diminished in Ag30 and Ag300, suggesting that the Ag NPs primarily comprised metallic phases. The surface atomic ratio (Ag/Ga + N) was calculated by integration of Ga $2p_{3/2}$, N 1s, and Ag 3d peaks followed by multiplying the atomic sensitivity factors of each element. The Ag/GaN ratios were 0.03, 0.22, and 1.05 for Ag3/GaN/Si, Ag30/GaN/Si, and Ag300/GaN/Si photoelectrodes, respectively (Figure 1h). This indicates an increasing surface coverage with higher $AgNO_3$ concentrations in the solution for the photodeposition.

2.2. PEC Urea Synthesis from NO_3^- and CO_2. Linear sweep voltammetry (LSV) measurements were carried out to investigate PEC urea synthesis in CO_2-saturated 0.5 M KNO_3 under AM 1.5 G 1 sun light illumination. The GaN/Si photoelectrode showed an onset potential (V_{onset}) = −0.3 V_{RHE}, where photocurrent density reaches −1 mA/cm^2 (Figure 2a). The V_{onset} was improved to −0.2 V_{RHE} after loading Ag NPs on the GaN/Si photoelectrode, indicating that metallic Ag promotes cathodic reactions such as urea synthesis, NO_3^- reduction, CO_2 reduction, or H_2 evolution. However, when too many Ag microplates were loaded (Ag300/GaN/Si), the photocurrent density rapidly decreased because the opaque Ag cocatalyst blocked the incident light and limited the number of photoexcited charge carriers in the GaN/Si photoelectrode. Under dark conditions, no measurable photocurrent density was observed in any of the samples, highlighting the requirement of solar light for the PEC reaction. The photocurrent utilization and product selectivity were investigated by measuring the faradaic efficiency (Figure 2b) and production rate of urea (Figure 2c) at −0.3 and −0.6 V_{RHE}. H_2 and CO gaseous products were measured by gas chromatograph, whereas urea, NH_3, N_2H_4, and NO_2^- liquid products were spectro-colorimetrically measured (Figure S6). Interestingly, all photoelectrodes produced very high FE_{urea} > 70% (Figure 2b) with a trace amount of NH_3, H_2, and CO products at −0.3 V_{RHE} (Figure S7). However, when operating at −0.6 V_{RHE}, there was a notable decline in the faradaic efficiency and production rate of urea on the GaN/Si and Ag3/GaN/Si photoelectrodes likely due to the insufficient surface coverage of Ag NPs. In contrast, Ag30/GaN/Si retained high selectivity >50% at −0.6 V_{RHE}. As a result, the Ag30/GaN/Si photoelectrode exhibited the highest production rate of urea at −0.6 V_{RHE} among the tested samples due to the optimized balance between catalytic activity and photocurrent generation (Figure 2c). It is noticed that the production rate of urea may be seemingly low, although most photogenerated electrons participated in urea synthesis because of the very large number of electrons (16-electron) involved in the urea synthetic reaction compared to the NH_3 synthesis from NO_3^- reduction (8-electron), CO production from CO_2 reduction (2-electron), and H_2 evolution (2-electron).

The potential-dependent FE of the product was measured and compared on GaN/Si and Ag/GaN/Si photoelectrodes. The GaN/Si photoelectrode exhibited high FE_{urea} > 70% at −0.3 and −0.4 V_{RHE} (Figure 2d). To the best of our knowledge, such high urea selectivity has never been reported among any known semiconductor materials and photoelectrodes. At more negative potentials (≤−0.5 V_{RHE}), NO_2^- was produced as the major product. The missing total FE (<20%) may be attributed to the presence of undetected byproducts, such as nitrogen, acetamide, and formamide.[46] Noticeably, Ag/GaN/Si showed a broader potential window (−0.1 to −0.6 V_{RHE}) for high FE_{urea} (Figure 2e). Ag/GaN/Si could achieve about a 4 times higher production rate of urea (4.4 ± 0.9 μmol/cm^2/h) than GaN/Si (1.0 ± 0.1 μmol/cm^2/h) at −0.6 V_{RHE} (Figure 2f) because the higher photocurrent density flows at more negative potentials. Ag NPs supported on GaN NWs have the clear advantages of improving the efficiency and productivity of urea synthesis. Owing to the built-in potential generated by solar light and the excellent catalytic selectivity, the Ag/GaN/Si photoelectrode showed high FE_{urea} = 75.6 ± 2.6% at a low potential of −0.3 V_{RHE} compared to previously reported electrocatalysts measured in dark conditions (Figure 2g and Table S1). While the potential required to achieve a high FE_{urea} of 75.6% is slightly more negative (−0.3 V_{RHE}) for the Ag/GaN/Si photoelectrode compared to the recent $CuWO_4$ electrocatalyst (FE_{urea} = 70.1% at −0.2 V_{RHE}), this suggests that the integration of high-performing cocatalysts with GaN NWs/n^+−p Si photoelectrodes has the potential to further shift the operating potential in a positive direction. Moreover, the stability of the Ag/GaN/Si photoelectrode was tested at −0.3 V_{RHE} for 6 cycles (Figure 2h). Each cycle was performed for 1 h. The electrolyte was replaced with a fresh one after the reaction. The photoelectrode consistently produced urea with a high FE_{urea} of 70.5 ± 5.0% and a production rate of 0.8 ± 0.1 μmol/cm^2/h, all while preserving its morphology (Figure S8) and chemical composition without any noticeable changes (Figure S9).

Control experiments were performed in three aqueous electrolytes of CO_2-saturated 0.5 M KNO_3, Ar-saturated 0.5 M KNO_3, and CO_2-saturated 0.5 M $KHCO_3$ to confirm that the C and N elements in urea originated from the CO_2 and NO_3^- sources, respectively. First, the GaN/Si photoelectrode (without Ag cocatalysts) showed more positive onset potential in the Ar-KNO_3 solution than the CO_2-KNO_3 solution, and a low current density <1 mA/cm^2 was measured in the CO_2-$KHCO_3$ solution within the potential up to −0.6 V_{RHE} (Figure 3a). This

https://doi.org/10.1021/acscatal.3c04264
ACS Catal. 2024, 14, 2588−2596

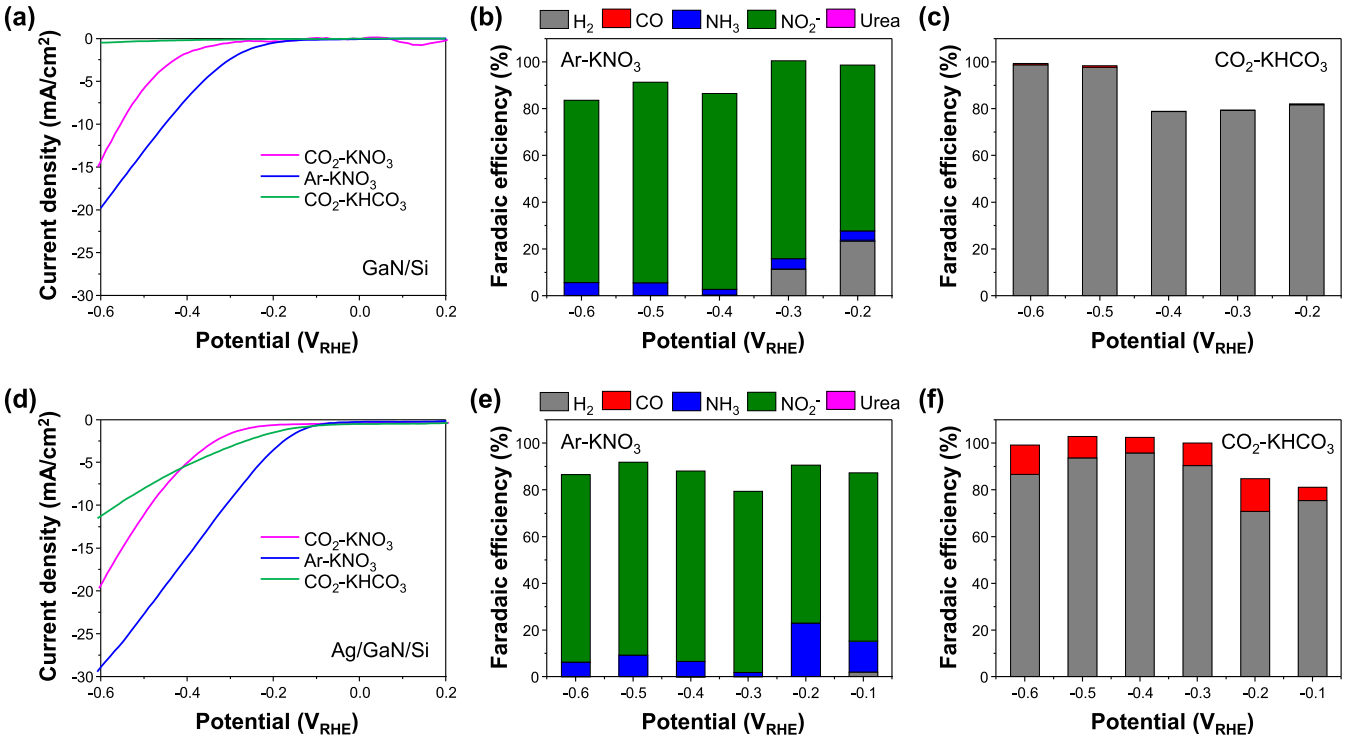

Figure 3. LSV curves of (a) GaN/Si and (d) Ag/GaN/Si measured in CO_2-saturated 0.5 KNO_3, Ar-saturated 0.5 M KNO_3 (Ar-KNO_3), and CO_2-saturated 0.5 M $KHCO_3$ (CO_2-$KHCO_3$). Faradaic efficiency of H_2, CO, NH_3, NO_2^-, and urea for GaN/Si in (b) Ar-KNO_3 and (c) CO_2-$KHCO_3$. Faradaic efficiency for Ag/GaN/Si in (e) Ar-KNO_3 and (f) CO_2-$KHCO_3$. Urea was not produced in either Ar-KNO_3 or CO_2-$KHCO_3$.

means that GaN is more selective for NO_3^- reduction reaction than CO_2 reduction and that CO_2 dissolved in the solution slows down the reaction kinetics likely due to lowering the local concentration of NO_3^- near the photoelectrode. Potential-dependent FEs were also measured in Ar-KNO_3 (Figure 3b) and CO_2-$KHCO_3$ (Figure 3c). In the Ar-KNO_3 solution, NO_2^- was the major product with $FE_{NO_2^-}$ > 70%, and minor products of H_2 and NH_3 were produced with FEs <20% (Figures 3b and S10a). In the CO_2-$KHCO_3$ solution, H_2 was the only product (Figures 3c and S10b). There was no CO evolution, despite the presence of the CO_2 reactant in the solution. These results reveal that GaN NWs can effectively reduce NO_3^- to NO_2^- but have no significant activity for the CO_2 reduction reaction. It should be noted that the GaN/Si photoelectrode, which cannot directly convert CO_2, selectively produced urea in the CO_2-KNO_3 electrolyte likely due to surface adsorbed intermediates such as *NO_2 that interact with CO_2 in the electrolyte and induce C−N coupling. This will be discussed in detail in the following section.

In stark contrast, Ag/GaN/Si showed improved LSV performance in the CO_2-$KHCO_3$ solution because the Ag catalyst is the well-known material for CO_2-to-CO conversion (Figure 3d).[47−49] Therefore, in the potential range of −0.1 to −0.6 V_{RHE}, where urea synthesis dominates in the CO_2-KNO_3 solution, there should be simultaneous reactions of NO_3^- reduction and CO_2 reduction. The selectivity of NO_3^- reduction was evaluated in the Ar-KNO_3 solution and it was found that most electrons were utilized for NO_2^- production and some were consumed for NH_3 synthesis (Figures 3e and S11a). There was no urea production, indicating that carbon from the CO_2 molecule should be provided to form the C−N bond. In the CO_2-$KHCO_3$ solution, H_2 was the dominant product but CO was also produced with a FE_{CO} of ∼12% and a production rate of ∼3.9 μmol/cm^2/h at −0.6 V_{RHE} (Figures 3f and S11b). The CO produced via CO_2 reduction reaction on the Ag/GaN/Si photoelectrode can react with N-containing intermediates (i.e., NO_2^- and NH_2) produced via NO_3^- reduction reaction, resulting in more efficient C−N coupling and urea synthesis as previously reported.[26,33] There was no urea production without the NO_3^- reactant in the electrolyte, confirming that urea is produced from both CO_2 and NO_3^- reactants. Furthermore, the isotope labeling test supported that NH_3, one of the products generated from NO_3^- reduction, indeed originated from NO_3^- in the electrolyte (Figure S12).

Inspired by Ag cocatalysts that can improve urea selectivity and productivity by enhancing CO generation, Au cocatalysts, known as efficient CO evolution catalysts,[50,51] were loaded onto GaN/Si photoelectrodes and tested as proof-of-concept experiments for PEC urea synthesis (Figure S13). The size of the Au NPs became larger as the precursor solution concentration increased from 6 to 600 μM. Similarly, the intensities of Ga $2p_{3/2}$ and N 1s XPS spectra gradually decreased and those of Au 4f XPS spectra increased with Au loading (Figure S14). Among the three photoelectrodes, Au60/GaN/Si showed the best LSV performance in CO_2-saturated 0.5 M KNO_3 due to the optimal surface coverage of Au NPs (Figure S15a). Au60/GaN/Si showed a high FE_{urea} = 76% at −0.2 V_{RHE} and a high production rate of urea = 2.1 μmol/cm^2/h at −0.6 V_{RHE}, which outperformed the GaN/Si photoelectrode and was slightly inferior to the Ag/GaN/Si photoelectrode (Figure S15b). However, as the applied potential was increased to −0.4 V_{RHE}, the Au/GaN/Si photoelectrode experienced a significant decrease in FE_{urea} to <1% and an increase in faradaic efficiency for NH_3 to 55% (Figure S16a,b). This suggests that Au NPs inherently have higher activity in converting NO_3^- to NH_3 compared to Ag

https://doi.org/10.1021/acscatal.3c04264
ACS Catal. 2024, 14, 2588−2596

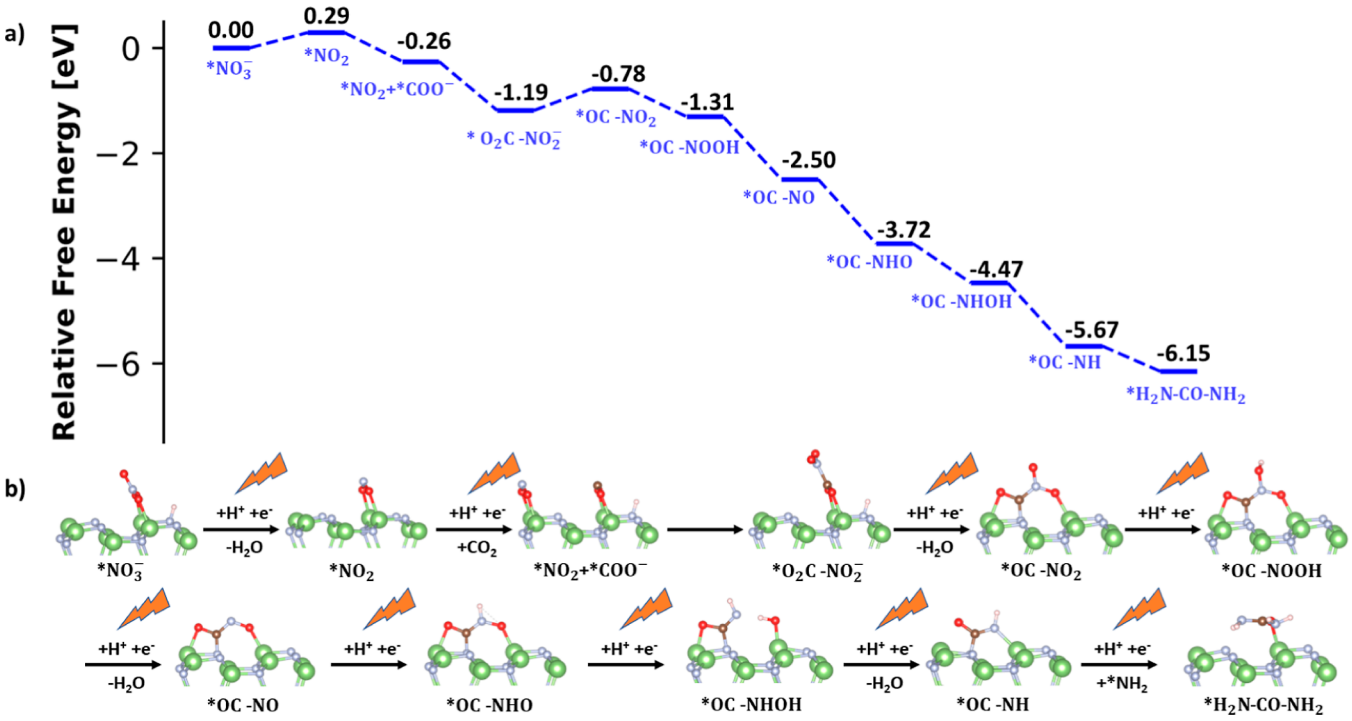

Figure 4. (a) Free energy profile of urea production on GaN without reduction of CO_2 to CO, including the crucial first step involving C−N bond formation, and subsequent reduction on the carbon site with further C−N bond formation and reduction. (b) DFT-optimized structures and reaction equations for each step.

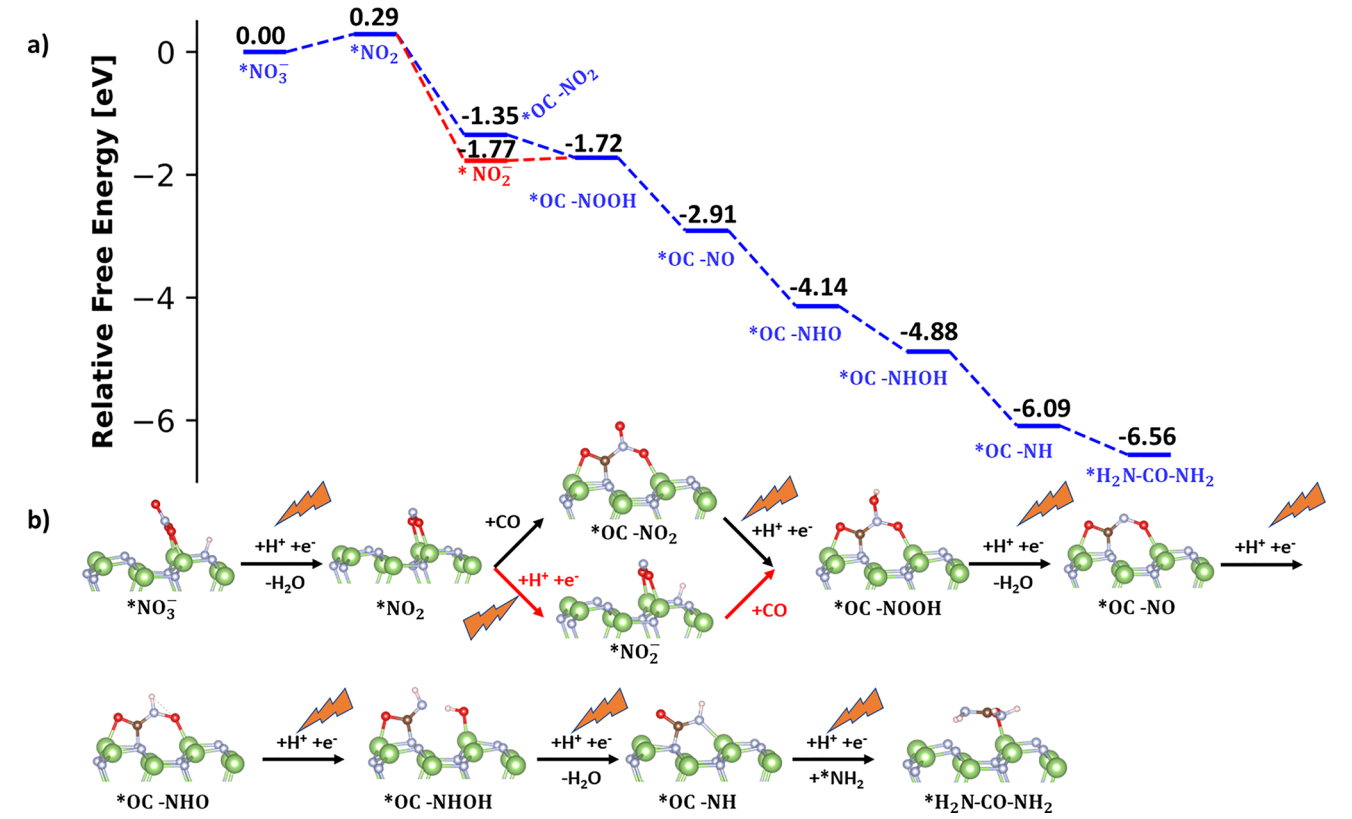

Figure 5. (a) Free energy profile of urea production on GaN with Ag particles. Ag particles reduce CO_2 to CO, so the C−N bond formation is facilitated by the reaction of CO with either $*NO_2$ (blue) or $*NO_2^-$ (red) intermediates. This is followed by further reduction and the second C−N bond formation. (b) Corresponding DFT-optimized structures and reaction equations for each step.

NPs, thereby resulting in a large deviation in urea production. The stability of Au NPs was confirmed by negligible degradation of FE_{urea} or the production rate during the 8 cycles of reaction (Figure S16c). Furthermore, Ag and Au

https://doi.org/10.1021/acscatal.3c04264
ACS Catal. 2024, 14, 2588−2596

cocatalysts were directly coated on the n^+−p Si photoelectrodes by photodeposition (Figure S17), and the PEC measurements were carried out in CO_2-saturated 0.5 M KNO_3 (Figure S18). Even with Ag and Au cocatalysts, the Si photoelectrodes exhibited very low photocurrent densities <0.7 mA/cm^2 (Figure S18a) and low selectivity of urea (FE_{urea} < 10% at −0.4 V_{RHE}) (Figure S18b), meaning that GaN NWs play a key role in reducing NO_3^- and stabilizing reaction intermediates for C−N coupling and consequent urea production.

2.3. Density Functional Theory Study on the Catalytic Mechanism. We have applied density functional theory (DFT) to investigate the catalytic mechanism of urea production from CO_2 and NO_3^-, with an emphasis on the key step associated with C−N bond formation and competing pathways on GaN (Figure S19). Formation of urea by the reduction of CO_2 and NO_3^- involves a 16-electron reaction with multiple steps along a complex reaction pathway (Figure 4). The crucial step is formation of the C−N bond, followed by subsequent reduction on the carbon site with further C−N bond formation and reduction. The relative energies of the reaction steps shown in Figure 4a correspond to the minimum energy structures shown in Figure 4b and are summarized in Table S2. The initial step of the mechanism involves adsorption of NO_3^- in a bidentate mode with two oxygens bound to adjacent gallium sites. NO_2 is formed on the surface upon the further reduction and release of a water molecule. At this stage, the NO_2 can either be reduced to NO_2^- or react with an adsorbed COO^- radical on the GaN surface (Figure 4b). Since both reactions are exergonic, the crucial C−N bond formation step proceeds in competition with formation of NO_2^- which can desorb from the surface or remain on the surface to be subsequently reduced to NH_3. After formation of the C−N bond, further reduction of the $O_2N{-}CO_2^-$ species is thermodynamically downhill (see also Figure S20). The second C−N bond formation involves the OC−NH intermediate and coadsorbed $*NH_2$. The resulting intermediate forms urea upon reduction. Therefore, after the first C−N coupling has taken place, formation of urea is energetically very favorable. We note that further reduction of NO_2^- to NO (and subsequent reduction to NH_3) is energetically uphill, making NO_2^- an important side product (Figure S21). Our calculations clearly show the negative potential that is needed to reduce CO_2 to CO on the GaN surface, in agreement with experimental results, while temporary production of the COO^- radical on the surface is thermodynamically favorable (Figure S22). Overall, our calculations suggest that the crucial step in urea production is the initial C−N bond formation that competes with NO_2^- formation since both reactions are exergonic (Figure S23). Remarkably, CO formation is disfavored, so the C−N coupling takes place between the coadsorbed NO_2 and COO^- through a radical coupling mechanism. Thus, stabilization of the COO^- radical on the GaN surface allows for C−N bond formation without forming CO as in electrochemical processes.

When a cocatalyst that can electrochemically reduce CO_2 to CO, such as Ag,[47−49] is present, the initial C−N bond formation is significantly facilitated, as shown in Figure 5. While the reduction to NO_2 and the formation of the second C−N bond remain the same, the initial coupling between carbon and nitrogen proceeds differently when CO is available. Since CO has weak adsorption on silver (Table S3, in agreement with references),[52,53] CO can approach the GaN surface and react with the adsorbed NO_2 intermediate to form the $O_2N{-}CO$ intermediate. In contrast to the coupling with COO^-, this facilitates urea production by making exergonic all subsequent catalytic steps after the NO_2. Additionally, C−N bond formation by reaction with the adsorbed NO_2^- intermediate is found to be thermodynamically accessible, although it did not react with CO_2. Therefore, the nitrite formation that leads to the main side product on GaN can still react by coupling to CO and form urea.

While C−N bond formation on GaN between adsorbed NO_2 and CO is favorable, it is unlikely on the Ag NPs, as shown in Figure S24. This is shown by the formation free energy of the $O_2N{-}CO$ intermediate from coadsorbed NO_2 and CO on a Ag(111) surface, which is the most common facet of the Ag NPs. Therefore, the Ag cocatalyst facilitates urea production by forming CO, as species that can diffuse toward the GaN and react with either NO_2 or NO_2^- intermediates adsorbed on the surface to form the C−N bond.

3. CONCLUSIONS

In summary, we have demonstrated an efficient GaN/Si photoelectrode for PEC urea synthesis from simultaneous NO_3^- and CO_2 reduction reactions under solar light. The built-in potential in n^+−p Si and the inherent catalytic activity of GaN NWs led to the selective synthesis of urea at a low overpotential. Moreover, Ag and Au cocatalysts loaded onto GaN NWs improved the performance of PEC urea synthesis, resulting in a high FE_{urea} of 75.6 ± 2.6% at a low potential of −0.3 V_{RHE}. This outperformed previous electrocatalysts measured under dark conditions. Theoretical calculation suggests that GaN NWs can convert NO_3^- to the NO_2 key intermediate, which then interacts with a COO^- radical on the surface, coupling carbon and nitrogen as the initial crucial step for urea production. This circumvents the need for initial CO formation. Our findings reveal that GaN decorated with cocatalysts has high catalytic activity for C−N coupling, which is a key step in the production of fertilizers. This finding suggests that GaN could be used to develop more efficient and sustainable methods of producing fertilizers.

■ ASSOCIATED CONTENT

Supporting Information

The Supporting Information is available free of charge at https://pubs.acs.org/doi/10.1021/acscatal.3c04264.

Experimental methods, figures showing characterization data, and tables showing performance of photoelectrodes (PDF)

■ AUTHOR INFORMATION

Corresponding Authors

Zetian Mi − *Department of Electrical Engineering and Computer Science, University of Michigan, Ann Arbor, Michigan 48109, United States;* orcid.org/0000-0001-9494-7390; Email: ztmi@umich.edu

Victor S. Batista − *Department of Chemistry, Yale University, New Haven, Connecticut 06520-8107, United States;* orcid.org/0000-0002-3262-1237; Email: victor.batista@yale.edu

Authors

Wan Jae Dong − *Department of Electrical Engineering and Computer Science, University of Michigan, Ann Arbor,*

Michigan 48109, United States; orcid.org/0000-0002-8520-5587

Jan Paul Menzel − *Department of Chemistry, Yale University, New Haven, Connecticut 06520-8107, United States;* orcid.org/0000-0002-1312-5000

Zhengwei Ye − *Department of Electrical Engineering and Computer Science, University of Michigan, Ann Arbor, Michigan 48109, United States*

Ishtiaque Ahmed Navid − *Department of Electrical Engineering and Computer Science, University of Michigan, Ann Arbor, Michigan 48109, United States;* orcid.org/0000-0001-6583-9331

Peng Zhou − *Department of Electrical Engineering and Computer Science, University of Michigan, Ann Arbor, Michigan 48109, United States*

Ke R. Yang − *Department of Chemistry, Yale University, New Haven, Connecticut 06520-8107, United States;* orcid.org/0000-0003-0028-2717

Complete contact information is available at: https://pubs.acs.org/10.1021/acscatal.3c04264

Author Contributions

[§]W.J.D. and J.P.M. contributed equally to this work.

Notes

The authors declare the following competing financial interest(s): Some IP related to this work was licensed to NS Nanotech, Inc. and NX Fuels, Inc., which were co-founded by Z. Mi. The University of Michigan and Mi have a financial interest in the companies.

■ ACKNOWLEDGMENTS

This work was supported by the United States Army Research Office Award W911NF2110337.

■ REFERENCES

(1) Lee, M.-Y.; Park, K. T.; Lee, W.; Lim, H.; Kwon, Y.; Kang, S. Current achievements and the future direction of electrochemical CO_2 reduction: A short review. *Crit. Rev. Environ. Sci. Technol.* **2020**, *50*, 769−815.

(2) Yoo, C. J.; Dong, W. J.; Park, J. Y.; Lim, J. W.; Kim, S.; Choi, K. S.; Odongo Ngome, F. O.; Choi, S.-Y.; Lee, J.-L. Compositional and geometrical effects of bimetallic Cu-Sn catalysts on selective electrochemical CO_2 reduction to CO. *ACS Appl. Energy Mater.* **2020**, *3*, 4466−4473.

(3) Kibria, M. G.; Edwards, J. P.; Gabardo, C. M.; Dinh, C. T.; Seifitokaldani, A.; Sinton, D.; Sargent, E. H. Electrochemical CO_2 reduction into chemical feedstocks: from mechanistic electrocatalysis models to system design. *Adv. Mater.* **2019**, *31*, 1807166.

(4) Fan, L.; Xia, C.; Yang, F.; Wang, J.; Wang, H.; Lu, Y. Strategies in catalysts and electrolyzer design for electrochemical CO_2 reduction toward C_2+ products. *Sci. Adv.* **2020**, *6*, No. eaay3111.

(5) Liu, H.; Wei, L.; Liu, F.; Pei, Z.; Shi, J.; Wang, Z.-j.; He, D.; Chen, Y. Homogeneous, heterogeneous, and biological catalysts for electrochemical N_2 reduction toward NH_3 under ambient conditions. *ACS Catal.* **2019**, *9*, 5245−5267.

(6) Wang, J.; Chen, S.; Li, Z.; Li, G.; Liu, X. Recent advances in electrochemical synthesis of ammonia through nitrogen reduction under ambient conditions. *ChemElectroChem* **2020**, *7*, 1067−1079.

(7) Chen, G. F.; Ren, S.; Zhang, L.; Cheng, H.; Luo, Y.; Zhu, K.; Ding, L. X.; Wang, H. Advances in electrocatalytic N_2 reduction—strategies to tackle the selectivity challenge. *Small Methods* **2019**, *3*, 1800337.

(8) Zeng, Y.; Priest, C.; Wang, G.; Wu, G. Restoring the nitrogen cycle by electrochemical reduction of nitrate: progress and prospects. *Small Methods* **2020**, *4*, 2000672.

(9) Wu, Z.-Y.; Karamad, M.; Yong, X.; Huang, Q.; Cullen, D. A.; Zhu, P.; Xia, C.; Xiao, Q.; Shakouri, M.; Chen, F.-Y.; et al. Electrochemical ammonia synthesis via nitrate reduction on Fe single atom catalyst. *Nat. Commun.* **2021**, *12*, 2870.

(10) Zhang, X.; Wang, Y.; Liu, C.; Yu, Y.; Lu, S.; Zhang, B. Recent advances in non-noble metal electrocatalysts for nitrate reduction. *Chem. Eng. J.* **2021**, *403*, 126269.

(11) van Langevelde, P. H.; Katsounaros, I.; Koper, M. T. Electrocatalytic nitrate reduction for sustainable ammonia production. *Joule* **2021**, *5*, 290−294.

(12) Soloveichik, G. Electrochemical synthesis of ammonia as a potential alternative to the Haber-Bosch process. *Nat. Catal.* **2019**, *2*, 377−380.

(13) Wang, P.; Chang, F.; Gao, W.; Guo, J.; Wu, G.; He, T.; Chen, P. Breaking scaling relations to achieve low-temperature ammonia synthesis through LiH-mediated nitrogen transfer and hydrogenation. *Nat. Chem.* **2017**, *9*, 64−70.

(14) Hao, D.; Chen, Z.-g.; Figiela, M.; Stepniak, I.; Wei, W.; Ni, B.-J. Emerging alternative for artificial ammonia synthesis through catalytic nitrate reduction. *J. Mater. Sci. Technol.* **2021**, *77*, 163−168.

(15) Ye, S.; Chen, Z.; Zhang, G.; Chen, W.; Peng, C.; Yang, X.; Zheng, L.; Li, Y.; Ren, X.; Cao, H.; et al. Elucidating the activity, mechanism and application of selective electrosynthesis of ammonia from nitrate on cobalt phosphide. *Energy Environ. Sci.* **2022**, *15*, 760−770.

(16) He, W.; Zhang, J.; Dieckhöfer, S.; Varhade, S.; Brix, A. C.; Lielpetere, A.; Seisel, S.; Junqueira, J. R.; Schuhmann, W. Splicing the active phases of copper/cobalt-based catalysts achieves high-rate tandem electroreduction of nitrate to ammonia. *Nat. Commun.* **2022**, *13*, 1129.

(17) Li, J.; Zhang, Y.; Kuruvinashetti, K.; Kornienko, N. Construction of C-N bonds from small-molecule precursors through heterogeneous electrocatalysis. *Nat. Rev. Chem* **2022**, *6*, 303−319.

(18) Chen, C.; He, N.; Wang, S. Electrocatalytic C-N coupling for urea synthesis. *Small Sci.* **2021**, *1*, 2100070.

(19) Tao, Z.; Rooney, C. L.; Liang, Y.; Wang, H. Accessing Organonitrogen Compounds via C-N Coupling in Electrocatalytic CO_2 Reduction. *J. Am. Chem. Soc.* **2021**, *143*, 19630−19642.

(20) Chen, C.; Zhu, X.; Wen, X.; Zhou, Y.; Zhou, L.; Li, H.; Tao, L.; Li, Q.; Du, S.; Liu, T.; et al. Coupling N2 and CO2 in H2O to synthesize urea under ambient conditions. *Nat. Chem.* **2020**, *12*, 717−724.

(21) Yuan, M.; Chen, J.; Bai, Y.; Liu, Z.; Zhang, J.; Zhao, T.; Wang, Q.; Li, S.; He, H.; Zhang, G. Unveiling Electrochemical Urea Synthesis by Co-Activation of CO_2 and N_2 with Mott-Schottky Heterostructure Catalysts. *Angew. Chem.* **2021**, *133*, 11005−11013.

(22) Mukherjee, J.; Paul, S.; Adalder, A.; Kapse, S.; Thapa, R.; Mandal, S.; Ghorai, B.; Sarkar, S.; Ghorai, U. K. Understanding the Site-Selective Electrocatalytic Co-Reduction Mechanism for Green Urea Synthesis Using Copper Phthalocyanine Nanotubes. *Adv. Funct. Mater.* **2022**, *32*, 2200882.

(23) Yuan, M.; Zhang, H.; Xu, Y.; Liu, R.; Wang, R.; Zhao, T.; Zhang, J.; Liu, Z.; He, H.; Yang, C.; et al. Artificial frustrated Lewis pairs facilitating the electrochemical N_2 and CO_2 conversion to urea. *Chem Catal.* **2022**, *2*, 309−320.

(24) Kayan, D. B.; Köleli, F. Simultaneous electrocatalytic reduction of dinitrogen and carbon dioxide on conducting polymer electrodes. *Appl. Catal., B* **2016**, *181*, 88−93.

(25) Huang, Y.; Yang, R.; Wang, C.; Meng, N.; Shi, Y.; Yu, Y.; Zhang, B. Direct Electrosynthesis of Urea from Carbon Dioxide and Nitric Oxide. *ACS Energy Lett.* **2022**, *7*, 284−291.

(26) Feng, Y.; Yang, H.; Zhang, Y.; Huang, X.; Li, L.; Cheng, T.; Shao, Q. Te-doped Pd nanocrystal for electrochemical urea production by efficiently coupling carbon dioxide reduction with nitrite reduction. *Nano Lett.* **2020**, *20*, 8282−8289.

(27) Meng, N.; Huang, Y.; Liu, Y.; Yu, Y.; Zhang, B. Electrosynthesis of urea from nitrite and CO_2 over oxygen vacancy-rich ZnO porous nanosheets. *Cell Rep. Phys. Sci.* **2021**, *2*, 100378.

(28) Cao, N.; Quan, Y.; Guan, A.; Yang, C.; Ji, Y.; Zhang, L.; Zheng, G. Oxygen vacancies enhanced cooperative electrocatalytic reduction of carbon dioxide and nitrite ions to urea. *J. Colloid Interface Sci.* **2020**, *577*, 109−114.
(29) Wei, X.; Wen, X.; Liu, Y.; Chen, C.; Xie, C.; Wang, D.; Qiu, M.; He, N.; Zhou, P.; Chen, W.; et al. Oxygen vacancy-mediated selective C-N coupling toward electrocatalytic urea synthesis. *J. Am. Chem. Soc.* **2022**, *144*, 11530−11535.
(30) Lv, C.; Zhong, L.; Liu, H.; Fang, Z.; Yan, C.; Chen, M.; Kong, Y.; Lee, C.; Liu, D.; Li, S.; et al. Selective electrocatalytic synthesis of urea with nitrate and carbon dioxide. *Nat Sustainability* **2021**, *4*, 868−876.
(31) Lv, C.; Lee, C.; Zhong, L.; Liu, H.; Liu, J.; Yang, L.; Yan, C.; Yu, W.; Hng, H. H.; Qi, Z.; et al. A Defect Engineered Electrocatalyst that Promotes High-Efficiency Urea Synthesis under Ambient Conditions. *ACS Nano* **2022**, *16*, 8213−8222.
(32) Saravanakumar, D.; Song, J.; Lee, S.; Hur, N. H.; Shin, W. Electrocatalytic conversion of carbon dioxide and nitrate ions to urea by a titania-Nafion composite electrode. *ChemSusChem* **2017**, *10*, 3999−4003.
(33) Meng, N.; Ma, X.; Wang, C.; Wang, Y.; Yang, R.; Shao, J.; Huang, Y.; Xu, Y.; Zhang, B.; Yu, Y. Oxide-Derived Core-Shell Cu@Zn Nanowires for Urea Electrosynthesis from Carbon Dioxide and Nitrate in Water. *ACS Nano* **2022**, *16*, 9095−9104.
(34) Zhang, X.; Zhu, X.; Bo, S.; Chen, C.; Qiu, M.; Wei, X.; He, N.; Xie, C.; Chen, W.; Zheng, J.; et al. Identifying and tailoring C-N coupling site for efficient urea synthesis over diatomic Fe-Ni catalyst. *Nat. Commun.* **2022**, *13*, 5337.
(35) Leverett, J.; Tran-Phu, T.; Yuwono, J. A.; Kumar, P.; Kim, C.; Zhai, Q.; Han, C.; Qu, J.; Cairney, J.; Simonov, A. N.; et al. Tuning the Coordination Structure of Cu-N-C Single Atom Catalysts for Simultaneous Electrochemical Reduction of CO_2 and NO_3^- to Urea. *Adv. Energy Mater.* **2022**, *12*, 2201500.
(36) Zhao, Y.; Ding, Y.; Li, W.; Liu, C.; Li, Y.; Zhao, Z.; Shan, Y.; Li, F.; Sun, L.; Li, F. Efficient urea electrosynthesis from carbon dioxide and nitrate via alternating Cu-W bimetallic C-N coupling sites. *Nat. Commun.* **2023**, *14*, 4491.
(37) Wu, Y.; Liu, X.; Pandey, A.; Zhou, P.; Dong, W. J.; Wang, P.; Min, J.; Deotare, P.; Kira, M.; Kioupakis, E.; et al. III-Nitride Nanostructures: Emerging Applications for Micro-LEDs, Ultraviolet Photonics, Quantum Optoelectronics, and Artificial Photosynthesis. *Prog. Quantum Electron.* **2022**, *85*, 100401.
(38) Vanka, S.; Arca, E.; Cheng, S.; Sun, K.; Botton, G. A.; Teeter, G.; Mi, Z. High efficiency Si photocathode protected by multifunctional GaN nanostructures. *Nano Lett.* **2018**, *18*, 6530−6537.
(39) Xiao, Y.; Vanka, S.; Pham, T. A.; Dong, W. J.; Sun, Y.; Liu, X.; Navid, I. A.; Varley, J. B.; Hajibabaei, H.; Hamann, T. W.; et al. Crystallographic Effects of GaN Nanostructures in Photoelectrochemical Reaction. *Nano Lett.* **2022**, *22*, 2236−2243.
(40) Yang, W.; Prabhakar, R. R.; Tan, J.; Tilley, S. D.; Moon, J. Strategies for enhancing the photocurrent, photovoltage, and stability of photoelectrodes for photoelectrochemical water splitting. *Chem. Soc. Rev.* **2019**, *48*, 4979−5015.
(41) Dong, W. J.; Navid, I. A.; Xiao, Y.; Lim, J. W.; Lee, J.-L.; Mi, Z. CuS-Decorated GaN Nanowires on Silicon Photocathodes for Converting CO_2 Mixture Gas to HCOOH. *J. Am. Chem. Soc.* **2021**, *143*, 10099−10107.
(42) Dong, W. J.; Navid, I. A.; Xiao, Y.; Lee, T. H.; Lim, J. W.; Lee, D.; Jang, H. W.; Lee, J.-L.; Mi, Z. Bi catalysts supported on GaN nanowires toward efficient photoelectrochemical CO_2 reduction. *J. Mater. Chem. A* **2022**, *10*, 7869−7877.
(43) Dong, W. J.; Zhou, P.; Xiao, Y.; Navid, I. A.; Lee, J.-L.; Mi, Z. Silver Halide Catalysts on GaN Nanowires/Si Heterojunction Photocathodes for CO_2 Reduction to Syngas at High Current Density. *ACS Catal.* **2022**, *12*, 2671−2680.
(44) Chang, X.; Wang, T.; Yang, P.; Zhang, G.; Gong, J. The development of cocatalysts for photoelectrochemical CO_2 reduction. *Adv. Mater.* **2019**, *31*, 1804710.
(45) Chelvayohan, M.; Mee, C. Work function measurements on (110),(100) and (111) surfaces of silver. *J. Phys. C: Solid State Phys.* **1982**, *15*, 2305−2312.
(46) Shin, S.; Sultan, S.; Chen, Z.-X.; Lee, H.; Choi, H.; Wi, T.-U.; Park, C.; Kim, T.; Lee, C.; Jeong, J.; et al. Copper with an atomic-scale spacing for efficient electrocatalytic co-reduction of carbon dioxide and nitrate to urea. *Energy Environ. Sci.* **2023**, *16*, 2003−2013.
(47) Dong, W. J.; Yoo, C. J.; Lim, J. W.; Park, J. Y.; Kim, K.; Kim, S.; Lee, D.; Lee, J.-L. Tailoring electronic structure of bifunctional Cu/Ag layered electrocatalysts for selective CO_2 reduction to CO and CH_4. *Nano Energy* **2020**, *78*, 105168.
(48) Dong, W. J.; Lim, J. W.; Hong, D. M.; Kim, J.; Park, J. Y.; Cho, W. S.; Baek, S.; Lee, J.-L. Grain Boundary Engineering of Cu-Ag Thin-Film Catalysts for Selective (Photo) Electrochemical CO_2 Reduction to CO and CH_4. *ACS Appl. Mater. Interfaces* **2021**, *13*, 18905−18913.
(49) Rosen, J.; Hutchings, G. S.; Lu, Q.; Rivera, S.; Zhou, Y.; Vlachos, D. G.; Jiao, F. Mechanistic insights into the electrochemical reduction of CO_2 to CO on nanostructured Ag surfaces. *ACS Catal.* **2015**, *5*, 4293−4299.
(50) Liu, M.; Pang, Y.; Zhang, B.; De Luna, P.; Voznyy, O.; Xu, J.; Zheng, X.; Dinh, C. T.; Fan, F.; Cao, C.; et al. Enhanced electrocatalytic CO_2 reduction via field-induced reagent concentration. *Nature* **2016**, *537*, 382−386.
(51) Chen, Y.; Li, C. W.; Kanan, M. W. Aqueous CO_2 reduction at very low overpotential on oxide-derived Au nanoparticles. *J. Am. Chem. Soc.* **2012**, *134*, 19969−19972.
(52) Hatsukade, T.; Kuhl, K. P.; Cave, E. R.; Abram, D. N.; Jaramillo, T. F. Insights into the electrocatalytic reduction of CO_2 on metallic silver surfaces. *Phys. Chem. Chem. Phys.* **2014**, *16*, 13814−13819.
(53) Jiang, T.; Mowbray, D.; Dobrin, S.; Falsig, H.; Hvolbæk, B.; Bligaard, T.; Nørskov, J. K. Trends in CO oxidation rates for metal nanoparticles and close-packed, stepped, and kinked surfaces. *J. Phys. Chem. C* **2009**, *113*, 10548−10553.

Recommended by ACS

Silver Metal–Organic Framework Derived N-Doped Carbon Nanofibers for CO_2 Conversion into β-Oxopropylcarbamates

Yu-Ting Zhai, Zhi-Lei Wu, *et al.*
JANUARY 24, 2024
INORGANIC CHEMISTRY
READ

Oxygen and Nitrogen Vacancies in a BiOBr/g-C_3N_4 Heterojunction for Sustainable Solar Ammonia Fertilizer Synthesis

Lei Zhang, Chengyin Wang, *et al.*
JANUARY 23, 2024
ACS SUSTAINABLE CHEMISTRY & ENGINEERING
READ

Opening Direct Electrochemical Fischer–Tropsch Synthesis Path by Interfacial Engineering of Cu Electrode with P-Block Elements

Ju Hyun Yang, Youngku Sohn, *et al.*
JANUARY 12, 2024
ACS APPLIED MATERIALS & INTERFACES
READ

Vacancy Optimized Coordination on Nickel Oxide for Selective Electrocatalytic Oxidation of Glycerol

Zhongcheng Xia, Yuqin Zou, *et al.*
JANUARY 22, 2024
ACS CATALYSIS
READ

Get More Suggestions >

https://doi.org/10.1021/acscatal.3c04264
ACS Catal. 2024, 14, 2588−2596